Understanding protein complex formation: the role of charge distribution in the encounter complex

Di Savino, A.

Chapter 4

Charge distribution on a protein surface determines whether productive or futile encounter complexes are formed.

Based on the research article:

Di Savino, A., Foerster, J, M., Ullmann, M., and Ubbink, M. Charge distribution on a protein surface determines whether productive or futile encounter complexes are formed. Biochemistry, 60(10), 747–755.

Abstract

Protein complex formation depends strongly on electrostatic interactions. The distribution of charges on the surface of redox proteins is often optimized by evolution to guide recognition and binding. To test to what degree the electrostatic interactions between cytochrome *c* peroxidase (CcP) and cytochrome *c* (Cc) are optimized, we produced five CcP variants, each with a different charge distribution on the surface. Monte Carlo simulations show that the addition of negative charges attracts Cc to the new patches, and the neutralization of the charges in the regular, stereospecific binding site for Cc abolishes the electrostatic interactions in that region entirely. For CcP variants with the charges in the regular binding site intact, additional negative patches slightly enhance productive complex formation, despite disrupting the optimized charge distribution. Removal of the charges in the regular binding site result in a dramatic decrease in the complex formation rate, even in the presence of highly negative patches elsewhere on the surface. It is concluded that additional charge patches can result in either productive or futile encounter complexes, depending on whether negative residues are located also in the regular binding site.

Chapter 4

Introduction

Protein complex formation proceeds through several steps. Freely diffusing proteins can collide and either move away again or form an encounter complex, which may or may not result in the formation of the stereospecific and active complex. The encounter complex is an ensemble of configurations in which the proteins sample each other's surface.[1] Formation is initially driven by electrostatic interactions but as the proteins get close, hydrophobic interactions can also come into play.[2–9] If the encounter results in the stereospecific complex, it is called productive, otherwise it is futile.[10,11] The rate of formation of the active complex defines association rate constant (k_a). If complex formation is not optimized, k_a can be four-five orders of magnitude lower than the number of collisions, because in most cases the proteins do not collide with binding sides oriented toward each other. Highly optimized protein complexes have k_a values close to the diffusion limit, due to strong electrostatic pre-orientation.[12] Harel *et al.* [10] studied complex formation of TEM1-β-lactamase (TEM1) and its inhibitor, β-lactamase-inhibitor protein (BLIP). They showed that charge mutations can enhance productive encounter complex formation, thus increasing the association rate without affecting the dissociation rate. However, other mutations modify the encounter complex without affecting the association rate or increase k_a without altering the encounter complex. The fractions of productive and futile encounter complexes can be altered with charge mutations on the proteins surface, even if they are far from the stereospecific binding site. By enhancing or disrupting a 'pathway' from the encounter site to the binding site in the stereospecific complex, they can either facilitate the formation of the active complex, or promote the early dissociation of the proteins.[13] The relation between productive vs. futile encounters and such electrostatic pathways on the protein surface was also suggested for the complex of cytochrome P450cam and putidaredoxin.[14] Despite their name, futile encounter complexes can have a role in protein functionality. Recently, it was shown that futile encounter complexes can regulate the activity of a protein complex through the formation of competitive encounters with a third protein.[15]

Electron transfer (ET) protein complexes are often highly optimized in complex formation and usually have a high fraction of encounter state. We selected the complex formed by cytochrome *c* (Cc) (CYC1, UniProtKB P00044) and cytochrome *c* peroxidase (CcP) (CCP1, UniProtKB P00431) to study the importance of the charge distribution on the protein surface in relation to rate of formation of the stereospecific complex. The protein complex formed by Cc and CcP has been extensively studied and has become a paradigm for biological ET. CcP catalyzes the reduction of H_2O_2 in yeast mitochondria through a cycle of reactions. The crystallographic structure of the complex with Cc published in 1992 represents the stereospecific complex,[16] and a second low-affinity binding site is present at ionic strength values below ~100 mM.[17–20] Electrostatic interactions are very important in the association reaction.[18,20–23] Erman and coworkers [24–26] measured the association rate between Cc and several charge-reversal mutants of CcP, showing that, interestingly, not

only residues close to the stereospecific binding site but also more distant ones have a role in the association. In a study from our groups, the charge distribution on the surface of CcP was changed strongly by addition of a negative patch on one side of CcP.[27] Monte Carlo simulations and paramagnetic relaxation enhancement (PRE) experiments showed that Cc interacts with the added patch, enlarging the surface visited in the encounter complex. The added charges also slightly enhance k_a. To investigate further to what degree the distribution of charges on the surface of CcP affects the association with Cc, here we analyze an additional four mutants of CcP with radically different charge distributions. Monte Carlo simulations show that the mutations alter the encounter complex, attracting Cc to the added negative patches. The association rates were measured through stopped flow experiments for a wide range of ionic strength values. Surprisingly, the added patches turn out to yield either productive or futile encounters, depending on whether the stereospecific site has its charges intact or not.

Results

Rearranging the CcP charge distribution creates new interactions sites.

Electrostatic interactions play an important role in the complex of Cc and CcP and appear to guide Cc to the binding site for fast electron transfer.[28–31] To test to what degree the electrostatic interactions are optimized for the association between Cc and CcP, we produced five CcP variants with a different charge distribution on their surface (Figure 4.1a,b). The CcP mutants were designed with three strategies, creation of an additional negative patch, neutralization of the negative charges in the wild type binding site for Cc, or a combination of both. Wild type CcP is named here CcP_A. In variants CcP_B and CcP_D an additional negative patch was introduced (charge change -8) on the side and the back of CcP, respectively. Variants CcP_C and CcP_E carry the same additional charges as CcP_B and CcP_D and have a +8 charge change around the stereospecific binding site as defined by the structures of the wild type complex determined by crystallography and NMR.[16,32] As a risult, CcP_C and CcP_E present a net charge change of zero. Finally, CcP_F only has the mutations in the stereospecific binding site, resulting a charge change of +8 and rendering CcP close to neutral. Some data on CcP_A and CcP_B were reported in a previous paper but are included here for completeness.[27]

Monte Carlo simulations in which Cc was docked on CcP a large number of times based solely on electrostatic interactions and steric constraints, showed that the negative charges introduced on the surface of CcP attract Cc to the new sites (Figure 4.1c). The new patches strongly attract Cc, both in CcP_B and CcP_D and this effect is further enhanced in CcP_C and CcP_E, suggesting that in all four mutants the encounter states would have Cc mostly or entirely at the new patches. Note that in the stereospecific complex next to electrostatic interactions, other favorable interactions are present in the WT type complex that are not modelled in these calculations, so it is expected that the shift in the interactions for the entire complex could be less than as shown in Figure 4.1c. For CcP_F, the calculations

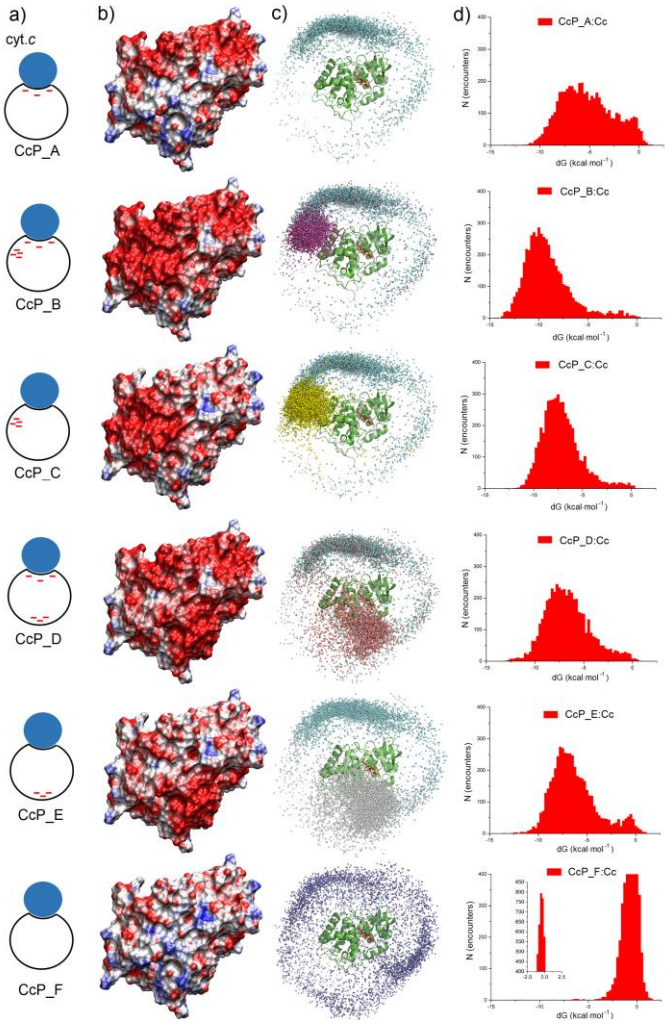

Figure 4.1. CcP variants. a) Schematic representation of the complexes formed by Cc and the CcP variants. Cc is represented as a blue circle bound at the stereospecific binding site and the CcP variants are represented as open circles with the negative charges on the surface indicated as red dashes; b) Electrostatic potential plotted on the surface of the CcP variants ranging from -5 (red) to 5 kcal/e^{o} (blue) at an ionic strength of 120 mM; c) The structure of CcP (green ribbon, heme in red) is surrounded by the centers of the mass of Cc in the ensemble of encounters of the complexes Cc:CcP_A (cyan), Cc:CcP_B (magenta), Cc:CcP_C (yellow), Cc:CcP_D (salmon), Cc:CcP_E (grey) and Cc:CcP_F (purple) as obtained from rigid body Monte Carlo simulations; d) Energy distribution of the encounter complexes between Cc and the CcP variants as obtained from rigid body Monte Carlo simulations. The inset shows the entire distribution for CcP_F using a different vertical scale.

show a more even distribution of Cc around CcP, as expected for a nearly neutral partner.

The energy distribution of the encounter complexes formed by the WT complex (Figure 4.1d) ranges from 0 to around -10 kcal/mol. The energy of most populated encounters is between about -4 to -7 kcal/mol; nevertheless a significant fraction of the encounters, around 25%, has an energy between -3 and 1 kcal/mol. The encounter complexes formed by Cc in presence of CcP_B, CcP_C, CcP_D, or CcP_E show that the encounters are distributed in more narrow peaks shifted to more negative energy compared to the WT encounter complexes, suggesting that they have a more favorable interactions than in Cc:CcP_A complex. In particular, the most favorable interactions are formed between Cc and CcP_B, with a peak at -10 kcal/mol. As expected, the least favorable encounters are formed by the Cc:CcP_F complex, which presents a very narrow peak centered on -0.5 kcal/mol.

CcP turnover involves two reduction steps.

Cc and CcP have high association (k_a) and dissociation (k_{-a}) rate constants: $k_a = 10^8 – 10^9$ $M^{-1}s^{-1}$ at 200 mM ionic strength,[33] $k_{-a} \geq 6{,}400$ s^{-1}.[27] The encounter complex represents 30% of the total complex,[30,32] the affinity is in the micromolar range (K_D = 5 μM),[34] and ET is fast (>50,000 s^{-1}).[35] To establish the effect of charge redistribution on the formation of the stereospecific, electron transfer active complex, the rate of oxidation of reduced Cc, Cc(Fe^{2+}), was measured for the different CcP variants. Stopped flow experiments were performed following the work by Miller *et al.* (1994).[33] Cc(Fe^{2+}) oxidation was followed by measuring the absorbance change at 416 nm over time in the cycle of reactions that allows CcP to reduce H_2O_2 to water. First, resting state CcP, CcP(Fe^{3+}), is reacted with hydrogen peroxide to create compound I (CpdI, reaction 1).[36–39] Then, after mixing with Cc(Fe^{2+}), a first molecule of Cc is oxidized to yield compound II (CpdII) and Cc(Fe^{3+}), reaction 2. A second Cc(Fe^{2+}) molecule can then reduce CpdII to resting state CcP, reaction 3.[40] Reactions 2 and 3 both contribute to the change in absorbance at 416 nm. Furthermore, a slow regain of absorbance was observed, which we attributed to dismutation of CpdII into CpdI and resting state CcP (reaction 4).

$$CcP(Fe^{3+}) + H_2O_2 \longrightarrow CpdI + H_2O \quad (1)$$

$$Cc(Fe^{2+}) + CpdI \xrightarrow{k(II)} Cc(Fe^{3+}) + CpdII \quad (2)$$

$$Cc(Fe^{2+}) + CpdII \xrightarrow{k(III)} Cc(Fe^{3+}) + CcP(Fe^{3+}) + H_2O \quad (3)$$

$$2CpdII \xrightarrow{k(IV)} CpdI + CcP(Fe^{3+}) \quad (4)$$

Immediately after mixing, reaction 2 dominates because the concentration of CpdI is maximal and that of CpdII still zero. Reaction 2 can be broken up in several steps, reaction 2a:

$$Cc(Fe^{2+}) + CpdI \underset{k_{-a}}{\overset{k_a}{\rightleftarrows}} Cc(Fe^{2+}){:}CpdI \xrightarrow{k_{et}} Cc(Fe^{3+}){:}CpdII \underset{k_d}{\overset{k_{-d}}{\rightleftarrows}} Cc(Fe^{3+}) + CpdII \qquad (2a)$$

The observed color change occurs after the electron transfer step (k_{et}) and thus the observed rate constant in the stopped-flow trace, k_{obs}, describes the first two parts of the reaction 2a. It can readily be shown that under pseudosteady state conditions ($\frac{\partial Cc(Fe2+):CpdI}{\partial t} = \frac{\partial Cc(Fe3+):CpdII}{\partial t} = 0$) equation (8) holds, giving the relation between the simulated rate *k(II)* and the association rate constant k_a:

$$k(II) = \frac{k_a k_{et}}{k_{-a} + k_{et}} \qquad (8)$$

To test whether the pseudosteady state assumption is applicable, the k_{obs} was obtained by fitting the initial part of the curve and the complete curve was simulated using differential equations that describe reaction (2) – (4), yielding estimates of the *k(II)*, *k(III)* and *k(IV)*. The two methods are illustrated in Figures 4.2 and S4.1. Note that the fitting method using the analytical solution given in equation 1 can be applied only at equal concentrations of Cc and CcP and it neglects reactions other than reaction 2, so it only fits the initial part of the decay (Figure 4.2). The remaining part is strongly affected by the other reactions. The simulation method covers the entire curve and has the advantage of not being limited to a specific ratio of concentrations between the proteins, enabling to evaluate the variation in the obtained rate due to concentration errors. This approach results in a more reliable error estimation for the rate constants. Excellent simulations could be obtained, but it should be noted that under some conditions there is some correlation between the obtained rate constants, so the three variables were not completely independent in all data sets (Table

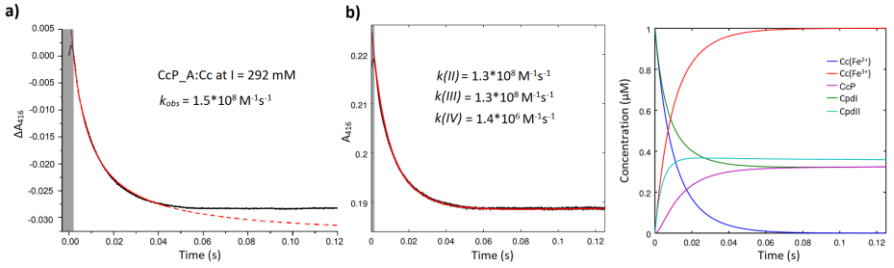

Figure 4.2. Comparison between fitting and simulation of the reaction performed by Cc and CcP_A at ionic strength 292 mM measured at the stopped flow. A grey area covers the first part of the measured data affected by a stopped flow artefact and thus excluded from the analysis. a) Fitting of the fast decay to equation 1 (see Materials and Methods in the Supplementary Information). The data are shown as a solid black line, the fit is represented by the red line. The extrapolation of the fit is shown as a dashed line. b) Left, simulation (red line) of the reactions 2-4 to fit the same data (black) as in panel (a). Right, the concentrations over time of all the species involved in the Cc:CcP cycle as derived from the simulation.

S4.3). Because of this correlation between parameters, we used simulations rather than fittings of the differential equations to avoid ending up in unrealistic local minima or with extreme values. For the analysis of the mutants, the primary interest is in *k(II)*. The values for this rate constant obtained by simulation matched the fitted k_{obs} values (Table S4.4), indicating that equation 8 is well approximated and *k(II)* can be used as a lower limit for the association rate constant k_a. For WT Cc and CcP, the electron transfer rate (k_{et}) is much larger than the dissociation rate constant (k_{-a}), so the observed rate constant approximates the association rate constant, $k(II) \approx k_a$.[12,41] In the remainder of the work, simulations were used for data analysis.

Cc association rates vary strongly for CcP variants

Due to the favorable electrostatic interactions between the Cc and CcP, the association rate constant for the WT proteins is high at low ionic strength and strongly decreases with increasing salt concentration (Figure 4.3).[18,20–23] It is estimated that at high salt concentration, at around 1.25 M ionic strength, all the mutants converge to the same k_a. At low salt concentration the complexes formed by Cc and the CcP variants A, B and D have a high k_a, likely to be very close to the diffusion limit (Figure 4.3). At ionic strength values between 292 mM and 622 mM (17 $mM^{1/2}$ - 25 $mM^{1/2}$ range on the horizontal scale in Figure

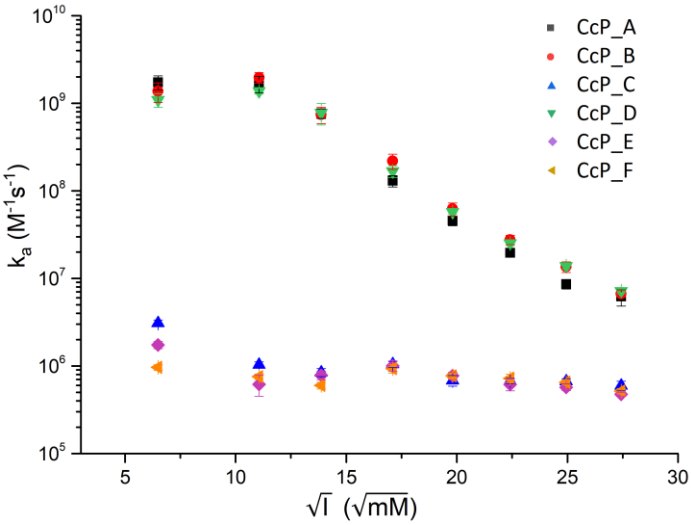

Figure 4.3. Rate of association (k_a) between Cc and the CcP variants. The k_a values, plotted as a function of the square root of the ionic strength, were obtained from the simulations of the stopped flow kinetics. Errors were calculated as the standard deviation between replicates and simulations performed at different CcP concentrations (see Materials and Methods in the Supplementary Information for details).

4.3) the association rate constant for Cc binding to CcP variant B is slightly higher than with CcP_A (Table S4.5). Similarly, CcP_D is slightly faster than CcP_A in the range 392 mM – 622 mM range of ionic strength. (Figure 4.3 and Table S4.5). Only at ionic strength values lower than 122 mM, the association with CcP_B and CcP_D is slightly slower than with the wild type CcP. The association rate constant for binding of Cc to CcP variants C, E and F is strongly reduced compared to that for the CcP_A. At ionic strength values higher than 170 mM (14 $mM^{1/2}$) the complexes formed by Cc and the mutants of CcP C and E show the same basal association rate as the complex formed with CcP_F. Only a significant difference is present at I = 44 mM (7 $mM^{1/2}$)(Table S4.5). In this condition the mutant CcP_C binds faster to Cc than CcP_E and CcP_F.

Discussion

To test the importance of the charge distribution on the surface of CcP for the interactions with Cc, five CcP mutants were created with different electrostatic potential and charge distribution on their surfaces (Figure 4.1.a, b). Monte Carlo simulations were performed for the wild type and mutated Cc:CcP complexes. The energy distributions for the Cc:CcP complexes (Figure 4.1d) show that the charge interactions between Cc and the CcP mutants, apart from the more neutral CcP_F, are more favorable than for the WT complex, in line with the increased overall negative charge on the mutants CcP_B and CcP_D. Interestingly, also mutants CcP_C and CcP_E, which have the same net charge as CcP_A, yield somewhat more favorable interactions. The reason could be that in the mutants an artificially highly negative patch is constructed. Often, charges on protein surfaces are compensated by nearby residues to ensure better protein stability. The simulations also demonstrate that these new patches strongly attract Cc, an effect that is enhanced further for the mutants in which the charges in the normal binding site are removed (CcP_C and CcP_E, Figure 4.1.c). Thus, it can be expected that the encounter complex of Cc and CcP is shifted toward binding at the new patches, which we demonstrated before for CcP_B using paramagnetic NMR spectroscopy.[27] In the Monte Carlo simulations it is assumed that all residues in the negative patches are charged but it cannot be excluded that mutual repulsion leads to increased pK_a values, rendering the patches with a lower net charge at the experimental pH value of 6.0. Furthermore, the simulations only consider electrostatic interactions and therefore neglect other favorable interactions that could play an important role at the stereospecific binding site. To determine whether productive complex formation, leading to ET from Cc to Cpd(I), can occur in the mutant complexes, stopped flow experiments were performed and association rate constants determined. The six CcP variants analyzed can be divided in two groups: CcP variants with the wild type charges in the binding site intact (CcP_A, CcP_B and CcP_D), and variants in which these charges were neutralized (CcP_E, CcP_C and CcP_F). The rate constants of association of the first group of CcP variants are similar and strongly dependent on the ionic strength due to the favorable electrostatic interactions between the Cc and CcP (Figure 4.3).[18,20–23] The second group instead presents a much lower association rate constant that is nearly independent of ionic strength. Clearly, the charges around the stereospecific binding site for Cc are

therefore fundamental for the formation of a productive encounter complex and efficient ET, in agreement with previous literature.[24–26] All variants of CcP bind the heme group, yielding similar UV-visible spectra as WT CcP, and they can all form CpdI and be reduced by Cc. Thus, the mutations do not affect the integrity of CcP. We cannot exclude however that the mutations around the stereospecific binding site subtly affect the protein surface, thus contributing to reduced formation of the ET active complex.

It can be expected that at high salt concentration, around 1.25 M ionic strength, all variants converge to the same basal association rate constant of ~5×10^5 M^{-1} s^{-1}, which is independent of ionic strength. The highest value observed, $k_a = 2 \times 10^9$ M^{-1} s^{-1}, shows that the electrostatic interactions can increase the rate 4000-fold compared to ET by random collision. The obtained rate constant *k(II)* is a lower limit estimate of k_a (equation 8), so the actual k_a could be even larger, but it seems to approach the diffusion limit, as is suggested by the leveling off of the k_a at very low ionic strength (Figure 4.3). Another explanation for such levelling off relates to the balance of monopole-dipole effects on the interactions as a function of ionic strength.[42–44]

The results indicate that the charges added on the surface of CcP_B and CcP_D do not negatively affect the formation of the stereospecific complex. We previously reported that the enlarged encounter region on CcP_B in fact slightly increases the association rate constant.[27] Our hypothesis is that the added charges enhance the electrostatic interactions between Cc and CcP, outweighing the negative effect of interacting at a site more distant from the stereospecific binding site. In other words, the additional charges enhance the probability of productive complex formation and binding at the new patch therefore, by definition, represent a productive encounter. Surprisingly, a similar result is observed with CcP_D. The association rate constants between Cc and CcP_D at ionic strength values between 392 mM and 622 mM (from 20 $mM^{1/2}$ to 25 $mM^{1/2}$) are significantly higher than the association measured for the wild type complex (Table S4.5). The differences are small for both CcP_B and CcP_D but are consistently higher than for CcP_A in that ionic strength range (Tables S4.5 and S4.6). The rigid-body Monte Carlo simulations shows that Cc is strongly attracted by the new negative patch of CcP_D, located on the opposite side of the protein with respect to the stereospecific binding site (Figure 4.1) and still it results in a slight increase in the rate of productive complex formation at moderate-high ionic strength values. Thus, analogous to CcP_B, it is concluded that the positive effect of the extra charges outweighs the remote binding relative to the reaction site, yielding more productive encounters for this variant. At ionic strength values lower than 122 mM (11 $mM^{1/2}$) the association rate constants between Cc and CcP_D is significantly lower than for the WT complex. This suggests that at low salt concentration the interaction between Cc and the new negative patch on CcP_D reduces the probability of Cc finding the stereospecific binding site. Similar biphasic behavior, with reduced ET rates at low ionic strength was reported before, for example for plastocyanin and plant cytochrome *f*.[45] Perhaps the most surprising result is that the new patches cannot compensate at all for the loss of the charge interactions at the stereospecific binding site. At ionic strength values

higher than 192 mM (14 $mM^{1/2}$) the complexes formed by Cc and CcP_C and CcP_E, which have a net charge identical to WT CcP, show the same, basal association rate constant as the complex formed with CcP_F, which has a charge change of +8 relative to WT CcP and is overall close to neutral. So, whereas the added charged patches appear to enhance the productive encounter formation in the presence of the charges in the stereospecific binding site, they have no effect on productive complex formation whatsoever if the binding site charges have been neutralized, at least at moderate and high ionic strength. An effect is only observed at 44 mM ionic strength (7 $mM^{1/2}$), at which condition the association rates constants show the order CcP_C > CcP_E > CcP_F. Apparently, at this salt concentration the electrostatic interactions are strong enough to result in slightly more productive encounters, with the largest effect for the charged patch that is closest to the stereospecific binding site (CcP_C). Similar results were obtained by Harel *et al.* [10] studying the complex formed by TEM1 and BLIP. Creating different mutants of BLIP and using stopped flow association rate measurements in combination with Brownian Dynamics simulations, they showed that increasing the number of charge interactions that led to successful binding (fruitful trajectories) increases the rate of association between the two proteins.

Conclusions

Our results indicate that in the presence of favorable charges in the binding site, the efficiency of the active protein complex formation depends more on the overall strength of the electrostatic interactions than on the distribution of charges on the protein surface. Nonetheless, the position of the charges on the protein surface can slightly affect productive complex formation, depending on the ionic strength conditions. At moderate and high ionic strength, additional charges enhance it, whereas at low ionic strength it can be reduced, as seen for CcP_D. The neutralization of the charges at the stereospecific binding site for Cc strongly affects the association of the two proteins, abolishing the electrostatic interactions entirely, as judged from the ionic strength independence of complex formation with CcP_F. Addition of highly charged patches distant from the stereospecific binding site only slightly enhances complex formation at low ionic strength and as no effect at moderate or high ionic strength. In this case, although the Monte Carlo simulations clearly show that electrostatic interactions are strong for CcP_C and CcP_E, apparently no trajectories are present for Cc to diffuse from the charged patch toward the stereospecific binding site, rather than to dissociate from CcP.[10,14] Therefore, in the absence of the negative charges in the stereospecific binding site, the encounters at the new patches have become futile ones.

References

(1) McLendon, G. (1991) Control of biological electron transport via molecular recognition and binding: The “velcro” model, in *Long-Range Electron Transfer in Biology*, p 159. Springer Berlin Heidelberg, Berlin, Heidelberg.

(2) Kim, Y. C., Tang, C., Clore, G. M., and Hummer, G. (2008) Replica exchange

simulations of transient encounter complexes in protein-protein association. *Proc. Natl. Acad. Sci. U. S. A. 105*, 12855–12860.

(3) Van de Water, K., van Nuland, N. A. J., and Volkov, A. N. (2014) Transient protein encounters characterized by paramagnetic NMR. *Chem. Sci. 5*, 4227–4236.

(4) Scanu, S., Foerster, J. M., Ullmann, G. M., and Ubbink, M. (2013) Role of hydrophobic interactions in the encounter complex formation of the plastocyanin and cytochrome *f* complex revealed by paramagnetic NMR spectroscopy. *J. Am. Chem. Soc. 135*, 7681–7692.

(5) Sugase, K., Dyson, H. J., and Wright, P. E. (2007) Mechanism of coupled folding and binding of an intrinsically disordered protein. *Nature 447*, 1021-U11.

(6) Camacho, C. J., Weng, Z., Vajda, S., and DeLisi, C. (1999) Free energy landscapes of encounter complexes in protein-protein association. *Biophys. J. 76*, 1166–1178.

(7) Camacho, C. J., Kimura, S. R., DeLisi, C., and Vajda, S. (2000) Kinetics of desolvation-mediated protein-protein binding. *Biophys. J. 78*, 1094–1105.

(8) Camacho, C. J., and Vajda, S. (2002) Protein-protein association kinetics and protein docking. *Curr. Opin. Struct. Biol. 12*, 36–40.

(9) Rajamani, D., Thiel, S., Vajda, S., and Camacho, C. J. (2004) Anchor residues in protein-protein interactions. *Proc. Natl. Acad. Sci. U. S. A. 101*, 11287–11292.

(10) Harel, M., Spaar, A., and Schreiber, G. (2009) Fruitful and futile encounters along the association reaction between proteins. *Biophys. J. 96*, 4237–4248.

(11) Fawzi, N. L., Doucleff, M., Suh, J. Y., and Clore, G. M. (2010) Mechanistic details of a protein-protein association pathway revealed by paramagnetic relaxation enhancement titration measurements. *Proc. Natl. Acad. Sci. U. S. A. 107*, 1379–1384.

(12) Schreiber, G., Haran, G., and Zhou, H. X. (2009) Fundamental aspects of protein-protein association kinetics. *Chem. Rev. 109*, 839–860.

(13) An, S. Y., Kim, E.-H., and Suh, J.-Y. (2018) Facilitated protein association via engineered target search pathways visualized by paramagnetic NMR spectroscopy. *Structure 26*, 887-893.e2.

(14) Andrałojć, W., Hiruma, Y., Liu, W. M., Ravera, E., Nojiri, M., Parigi, G., Luchinat, C., and Ubbink, M. (2017) Identification of productive and futile encounters in an electron transfer protein complex. *Proc. Natl. Acad. Sci. U. S. A. 114*, E1840–E1847.

(15) Strickland, M., Kale, S., Strub, M. P., Schwieters, C. D., Liu, J., Peterkofsky, A., and Tjandra, N. (2019) Potential regulatory role of competitive encounter complexes in paralogous phosphotransferase systems. *J. Mol. Biol. 431*, 2331–2342.

(16) Pelletier, H., and Kraut, J. (1992) Crystal structure of a complex between electron transfer partners, cytochrome *c* peroxidase and cytochrome *c*. *Science (80). 258*, 1748–1755.

(17) Stemp, E. D. A., and Hoffman, B. M. (1993) Cytochrome *c* peroxidase binds two molecules of cytochrome *c*: evidence for a low-affinity, electron-transfer-active site on

cytochrome *c* peroxidase. *Biochemistry 32*, 10848–10865.

(18) Zhou, J. S., and Hoffman, B. M. (1994) Stern-Volmer in reverse - 2/1 stoichiometry of the cytochrome *c* cytochrome *c* peroxidase electron-transfer complex. *Science (80). 265*, 1693–1696.

(19) Mauk, M. R., Ferrer, J. C., and Mauk, A. G. (1994) Proton linkage in formation of the cytochrome *c*-cytochrome *c* peroxidase complex: Electrostatic properties of the high- and low-affinity cytochrome binding sites on the peroxidase. *Biochemistry 33*, 12609–12614.

(20) Van de Water, K., Sterckx, Y. G. J., and Volkov, A. N. (2015) The low-affinity complex of cytochrome *c* and its peroxidase. *Nat. Commun. 6*, 7073.

(21) Matthis, A. L., and Erman, J. E. (1995) Cytochrome *c* peroxidase-catalyzed oxidation of yeast iso-1 ferrocytochrome *c* by hydrogen peroxide. Ionic strength dependence of the steady-state parameters. *Biochemistry 34*, 9985–9990.

(22) Matthis, A. L., Vitello, L. B., and Erman, J. E. (1995) Oxidation of yeast iso-1 ferrocytochrome *c* by yeast cytochrome *c* peroxidase compounds I and II. Dependence upon ionic strength. *Biochemistry 34*, 9991–9999.

(23) McLendon, G., Zhang, Q., Billstone, V., Wallin, S. A., Miller, R. M., Spears, K. G., and Hoffman, B. M. (1993) Thermodynamic and kinetic aspects of binding and recognition in the cytochrome c/cytochrome c peroxidase complex. *J. Am. Chem. Soc. 115*, 3665–3669.

(24) Erman, J. E., Vitello, L. B., Pearl, N. M., Jacobson, T., Francis, M., Alberts, E., Kou, A., and Bujarska, K. (2015) Binding of yeast cytochrome *c* to forty-four charge-reversal mutants of yeast cytochrome *c* peroxidase: isothermal titration calorimetry. *Biochemistry 54*, 4845–4854.

(25) Pearl, N. M., Jacobson, T., Arisa, M., Vitello, L. B., and Erman, J. E. (2007) Effect of single-site charge-reversal mutations on the catalytic properties of yeast cytochrome *c* peroxidase: Mutations near the high-affinity cytochrome *c* binding site. *Biochemistry 46*, 8263–8272.

(26) Pearl, N. M., Jacobson, T., Meyen, C., Clementz, A. G., Ok, E. Y., Choi, E., Wilson, K., Vitello, L. B., and Erman, J. E. (2008) Effect of single-site charge-reversal mutations on the catalytic properties of yeast cytochrome *c* peroxidase: Evidence for a single, catalytically active, cytochrome *c* binding domain. *Biochemistry 47*, 2766–2775.

(27) Di Savino, A., Foerster, J., La Haye, T., Blok, A., Timmer, M., Ullmann, M., and Ubbink, M. (2020) Efficient encounter complex formation and electron transfer to cytochrome *c* peroxidase with an additional, distant electrostatic binding site. *Angew. Chemie Int. Ed. 132*, 23239–23243.

(28) Gabdoulline, R. R., and Wade, R. C. (2001) Protein-protein association: investigation of factors influencing association rates by Brownian dynamics simulations. *J. Mol. Biol. 306*, 1139–1155.

(29) Northrup, S. H., Boles, J. O., and Reynolds, J. C. (1988) Brownian dynamics of cytochrome *c* and cytochrome *c* peroxidase association. *Science (80-.). 241*, 67–70.

(30) Bashir, Q., Volkov, A. N., Ullmann, G. M., and Ubbink, M. (2010) Visualization of the encounter ensemble of the transient electron transfer complex of cytochrome *c* and cytochrome *c* peroxidase. *J. Am. Chem. Soc. 132*, 241–247.

(31) Castro, G., Boswell, C. A., and Northrup, S. H. (1998) Dynamics of protein-protein docking: Cytochrome *c* and cytochrome *c* peroxidase revisited. *J. Biomol. Struct. Dyn. 16*, 413–424.

(32) Volkov, A. N., Worrall, J. A. R., Holtzmann, E., and Ubbink, M. (2006) Solution structure and dynamics of the complex between cytochrome *c* and cytochrome *c* peroxidase determined by paramagnetic NMR. *Proc. Natl. Acad. Sci. U. S. A. 103*, 18945–18950.

(33) Miller, M. A., Liu, R. Q., Hahm, S., Geren, L., Hibdon, S., Kraut, J., Durham, B., and Millett, F. (1994) Interaction domain for the reaction of cytochrome *c* with the radical and the oxyferryl heme in cytochrome *c* peroxidase compound I. *Biochemistry 33*, 8686–8693.

(34) Worrall, J. A. R., Kolczak, U., Canters, G. W., and Ubbink, M. (2001) Interaction of yeast iso-1-cytochrome *c* with cytochrome *c* peroxidase investigated by N-15,H-1 heteronuclear NMR spectroscopy. *Biochemistry 40*, 7069–7076.

(35) Geren, L., Hahm, S., Durham, B., and Millett, F. (1991) Photoinduced electron-transfer between cytochrome *c* peroxidase and yeast cytochrome *c* labeled at cys-102 with(4-bromomethyl-4'-methylbipyridine) bis(bypyridine) ruthenium^{2+}. *Biochemistry 30*, 9450–9457.

(36) Mauro, J. M., Fishel, L. A., Hazzard, J. T., Meyer, T. E., Tollin, G., Cusanovich, M. A., and Kraut, J. (1988) Tryptophan-191→ Phenylalanine, a proximal-side mutation in yeast cytochrome *c* peroxidase that strongly affects the kinetics of ferrocytochrome *c* oxidation. *Biochemistry 27*, 6243–6256.

(37) Sivaraja, M., Goodin, D. B., Smith, M., and Hoffman, B. M. (1989) Identification by ENDOR of Trp191 as the free-radical site in cytochrome *c* peroxidase compound ES. *Science (80-.). 245*, 738–740.

(38) Erman, J. E., Vitello, L. B., Mauro, J. M., and Kraut, J. (1989) Detection of an oxyferryl porphyrin π-cation-radical intermediate in the reaction between hydrogen peroxide and a mutant yeast cytochrome *c* peroxidase. Evidence for tryptophan-191 involvement in the radical site of compound. *Biochemistry 28*, 7992–7995.

(39) Fishel, L. A., Farnum, M. F., Miller, M. A., Kraut, J., Mauro, J. M., Liu, Y., Tan, X. ling, and Scholes, C. P. (1991) Compound I radical in site-directed mutants of cytochrome *c* peroxidase as probed by electron paramagnetic resonance and electron-nuclear double resonance. *Biochemistry 30*, 1986–1996.

(40) Kim, K. L., Kang, D. S., Vitello, L. B., and Erman, J. E. (1990) Cytochrome *c* peroxidase catalyzed oxidation of ferrocytochrome *c* by hydrogen-peroxide - Ionic-strenght dependence of the steady-state rate parameters. *Biochemistry 29*, 9150–9159.

(41) Ho, P. S., Hoffman, B. M., Solomon, N., Kang, C. H., and Margoliash, E. (1984) Kinetics and energetics of intramolecular electron-transfer in yeast cytochrome *c* peroxidase. *Biochemistry 23*, 4122–4128.

(42) Koppenol, W. H., and Margoliash, E. (1982) The asymmetric distribution of charges on the surface of horse cytochrome c - Functional implications. *J. Biol. Chem. 257*, 4426–4437.

(43) Van Leeuwen, J. W. (1983) The ionic strength dependence of the rate of a reaction between two large proteins with a dipole moment. *Biochim. Biophys. Acta - Protein Struct. Mol. Enzymol. 743*, 408–421.

(44) Watkins, J. A., Cusanovich, M. A., Meyer, T. E., and Tollin, G. (1994) A "parallel plate" electrostatic model for bimolecular rate constants applied to electron transfer proteins. *Protein Sci. 3*, 2104–2114.

(45) Meyer, T. E., Zhao, Z. G., Cusanovich, M. A., and Tollin, G. (1993) Transient kinetics of electron transfer from a variety of *c*-type cytochromes to plastocyanin. *Biochemistry 32*, 4552–4559.

Supplementary Information:

Materials and Methods

Mutagenesis

The *Saccharomyces cerevisiae* CcP (CCP1, UniProtKB P00431) considered WT in this study (CcP_A) contains the mutation C128A to avoid dimerization and the additional sequence MKT at the N-terminus for enhanced production levels.[1,2] The gene was subcloned into a pET2a(+) vector.[3] CcP_B additionally has the mutations K21E, K29E, K90E, and K97E; [4] CcP_C contains the same mutations as in CcP_B and D35N, E36Q, E119Q, E202Q, E210Q, E215Q, D225N and E291Q that neutralize the charges of the WT binding site; CcP_D has mutations K75E, K76Q, N79D, Q87E, K91Q, K98Q, N142D in comparison to CcP_A; CcP_E has the same mutations as in mutant CcP_D and the mutations that neutralize the charges of the WT binding site as in CcP_C; CcP_F only has the neutralization charges for the WT binding site (See Table S4.1). The DNA constructs were produced by a commercial company and verified by DNA sequencing.

Protein Production

CcP was expressed in *Escherichia coli* BL21 Star (DE3)pLysS (Life Technologies Europe BV, Bleiswijk, the Netherlands). The production and purification were performed as previously described[1,3,5] with some differences according to the CcP variant purified. Buffers with different ionic strength values were used to build the gradient for elution during the anion-exchange chromatography; 50 mM potassium phosphate pH 5 and 500 mM potassium phosphate pH 5 for CcP_A and CcP_C and CcP_E; 500 mM KCl was added to the second buffer to elute CcP_B and CcP_D. The purification of CcP_F comprised a precipitation step with 40% w/w ammonium sulphate at 25°C, followed by dialysis against 20 mM potassium phosphate pH 5 overnight. Finally, the sample was loaded on an SP column, the column was washed with 20 mM potassium phosphate pH 5 and eluted with 20 column volumes of a gradient to 20 mM potassium phosphate and 1 M NaCl, pH 5. *S. cerevisiae* Cc (CYC1, UniProtKB P00044) was expressed using the iso-1-cytochrome *c* gene in a pUC19 based plasmid and purified following the protocols previously described.[3,6]

Monte Carlo simulations

The structures were prepared and the Monte Carlo docking simulations were done as described in Di Savino *et al*. (2020)[4]. The structures of CcP and Cc from the PDB 2PCC[7] were used as basis for the simulations. The hydrogens of the proteins were added with HBUILD[8] in CHARMM[9] and minimized with the CHARMM force field[10], while the heavy atoms were fixed. The HEME ligands within the protein were considered to be in the oxidized state. For each version of CcP (CcP_A – CcP_F) the mutations, described in the Mutagenesis section, were introduced using Pymol[11]. The electrostatic potential was

calculated with APBS[12] for each CcP mutant separately. The potential was calculated in the presence of 120 mM NaCl and at a temperature of 303 K. The Monte Carlo docking simulations were done with the program suite MCMap[13]. Separate simulations were done for each CcP mutant considering its respective electrostatic potential. In the simulation, Cc (ligand) moves randomly in the electrostatic potential of CcP (receptor). From each simulation, 5000 randomly chosen encounters were used for further analysis. A protein pair Cc:CcP was considered as encounter complex if the distance between at least two atoms of each protein respectively was less than 3 Å.

Kinetic measurements

The results of the kinetics measured for the Cc:CcP_A and Cc:CcP_B complexes at ionic strengths from 752 mM to 122 mM were presented in our previous work.[4] The same protocols were followed to measure the reactions between Cc and the other mutants of CcP. The kinetic measurements were performed at the ionic strengths 752 mM, 622 mM, 502 mM, 392 mM, 292 mM, 192 mM, 122 mM and 44 mM on a SX20 stopped flow spectrometer (AppliedPhotophysics, Leatherhead, Surrey, UK) with a 1.2 ms deadtime at room temperature following the absorbance at 416 nm, which indicates oxidation of Cc.[14] Equimolar solutions of Cc and CcP were mixed to a final concentration of 0.5 µM of both Cc and CcP.

Kinetic data analysis

The stopped flow data were fitted to the equation 1 as previously described:[4]

$$\Delta A_{416} = B_0 \cdot \Delta\varepsilon_{416} \cdot \left(1 - \frac{1}{1+k_{obs} \cdot B_0 \cdot t}\right) + C \qquad (1)$$

where B_0 is the starting concentration of $Cc(Fe^{2+})$ and CpdI after mixing, $\Delta\varepsilon_{416}$ is the difference in extinction coefficient at 416 nm for oxidized and reduced Cc, -40 mM^{-1} cm^{-1} ([15–17]), k_{obs} (s^{-1}) is the observed rate constant of reduction, t is time (s) and C corrects for the baseline voltage of the spectrometer.

An independent analysis of the stopped flow data was performed through simulations. Kinetic simulations using GNU Octave[18] were performed to simulate the experimental measurement of the kinetics obtained from a stopped flow measurement. The script is included in Script S4.1. To do so, the reactions 2, 3 and 4 (see Results section) that influence the absorbance at 416 nm during the catalytic cycle were considered. The following differential equations were used to describe the change in concentration of each species in solution during the cycle:

$$\frac{d[Cc(Fe^{2+})]}{dt} = -k(II) * [Cc(Fe^{2+})] * [CpdI] - k(III) * [Cc(Fe^{2+})] * [CpdII]; \qquad (2)$$

$$\frac{d[CpdI]}{dt} = -k(II) * [Cc(Fe^{2+})] * [CpdI] + k(IV) * [CpdII]^2; \qquad (3)$$

$$\frac{d[Cc(Fe^{3+})]}{dt} = k(II) * [Cc(Fe^{2+})] * [CpdI] + k(III) * [Cc(Fe^{2+})] * [CpdII]; \quad (4)$$

$$\frac{d[CpdII]}{dt} = k(II) * [Cc(Fe^{2+})] * [CpdI] - k(III) * [Cc(Fe^{2+})] * [CpdII] - k(IV) * [CpdII]^2; \quad (5)$$

$$\frac{d[CcP]}{dt} = k(IV) * [CpdII]^2 + k(III) * [Cc(Fe^{2+})] * [CpdII]; \quad (6)$$

From the simulated concentrations the stopped flow trace is recreated by summing the contributions of each component to the absorbance at 416 nm following the Beer-Lambert law:

$$A_{416} = \varepsilon_{Cc(Fe2+)} * [Cc(Fe^{2+})] + \varepsilon_{CpdI} * [CpdI] + \varepsilon_{Cc(Fe3+)} * [Cc(Fe^{3+})] + \varepsilon_{CpdII} * [CpdII] + \varepsilon_{CcP} * [CcP] + C \quad (7)$$

The extinction coefficients at 416 nm are 129.1 $mM^{-1}cm^{-1}$ for $Cc(Fe^{2+})$,[19] 88.8 $mM^{-1}cm^{-1}$ for $Cc(Fe^{3+})$,[19] and for CcP and CpdI according to Table S4.2. The extinction coefficient for CdpII was considered to be the same as for the corresponding CpdI. The baseline correction term C was optimized manually (variable prod in the script S4.1 in the supporting information). The values of *k(II)*, *k(III)* and *k(IV)* were independently changed until the simulation was a good fit as judged by visual inspection. The main error for the stopped flow measurement is caused by the error in the concentration of Cc and CpdI. Repeated measurement of the concentration of the samples resulted in a maximum deviation of 20% from the theoretical one. To take this into account in the simulations, every kinetic measurement, consisting of at least three replicates per salt concentration, was simulated at the expected experimental concentration, and at a concentration of CcP 20% lower. The rates of the reactions at a particular salt concentration were calculated as the average of the values obtained from the single simulations. The error of the rates at each salt concentration were calculated as the standard deviation between the rates at different protein concentrations. A t-test was performed to verify whether differences between the association rates of the Cc:CcP complexes are statistically significant. The Bonferroni correction with n = 5 was applied when comparing the data of a CcP variant with the other five variants (Tables S4.5 and S4.6). The analysis of the data suggests that dismutation of CpdII (reaction 4) is much slower than the other reactions. Nonetheless, the occurrence of this reaction explains the increase of the absorbance at 416 nm visible in kinetic traces obtained at low ionic strength.

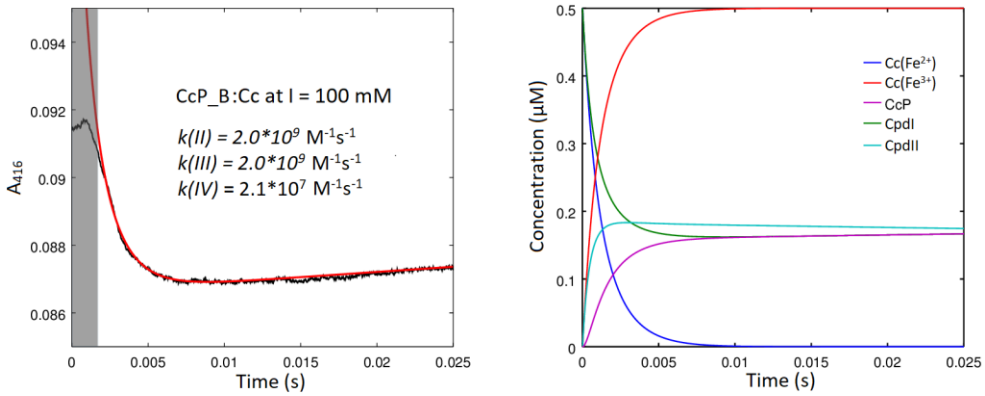

Figure S4.1. Example of kinetics measured at low ionic strength. In the panel on the left the experimental data is shown in black, the simulation in red. The first part of the data is affected by an artefact of the stopped flow and thus excluded from the analysis and is shown in a grey area. In the panel on the right the concentrations of all the species involved in the Cc:CcP cycle are shown as a function of time based on the simulated data.

Table S4.1. List of mutations performed for each CcP variant.

CcP_A	C128A
CcP_B	C128A, K21E, K29E, K90E, K97E
CcP_C	C128A, K21E, K29E, K90E, K97E, D35N, E36Q, E119Q, E202Q, E210Q, E215Q, D225N, E291Q
CcP_D	C128A, K75E, K76Q, N79D, Q87E, K91Q, K98Q, N142D
CcP_E	C128A, K75E, K76Q, N79D, Q87E, K91Q, K98Q, N142D, D35N, E36Q, E119Q, E202Q, E210Q, E215Q, D225N, E291Q
CcP_F	C128A, D35N, E36Q, E119Q, E202Q, E210Q, E215Q, D225N, E291Q

Table S4.2. Extinction coefficients for the CcP variants and their CpdIs at ionic strengths from 44 mM to 752 mM. The extinction coefficients are in mM^{-1} cm^{-1}. The error is estimated to be ± 5 %.

		CcP_A	CcP_B	CcP_C	CcP_D	CcP_E	CcP_F
44 mM	**CcP**	92	87	88	75	73	80
	CpdI	101	96	99	95	95	92
122 mM	**CcP**	106	94	103	103	103	99
	CpdI	113	80	117	119	122	87
192 mM	**CcP**	104	94	100	82	75	88
	CpdI	97	91	99	96	96	88
292 mM	**CcP**	108	94	98	78	75	93
	CpdI	95	91	98	94	94	92
392 mM	**CcP**	117	94	103	78	77	99
	CpdI	94	80	85	95	93	97
502 mM	**CcP**	117	94	114	86	84	99
	CpdI	97	80	105	105	100	87
622 mM	**CcP**	114	94	109	81	78	85
	CpdI	99	80	95	96	94	89
752 mM	**CcP**	112	94	102	82	80	99
	CpdI	94	80	102	96	93	87

Table S4.3. Rate constants k(II), k(III) and k(IV) ($M^{-1}s^{-1}$) obtained by simulation of the entire cycle of reactions for the six CcP variants to match the experimental data curves. The error is calculated as standard deviation between the rates obtained by simulations of at least three single measurements at each ionic strength value. The highlighted values are outliers that are not compatible with our model.

			CcP_A			
I (mM)	**k(II)**	**st.dev.**	**k(III)**	**st.dev.**	**k(IV)**	**st.dev.**
44	1.7E+09	3.2E+08	1.7E+09	3.2E+08	1.3E+07	4.7E+06
122	1.7E+09	3.6E+08	1.7E+09	3.6E+08	1.5E+07	6.5E+06
192	7.7E+08	9.7E+07	7.7E+08	9.7E+07	4.3E+07	1.8E+07
292	1.3E+08	1.9E+07	1.3E+08	1.9E+07	1.4E+06	9.6E+05
392	4.6E+07	5.8E+06	4.5E+07	6.5E+06	4.0E+05	1.9E+05
502	2.0E+07	2.0E+06	1.6E+07	7.8E+06	2.2E+05	1.1E+05
622	8.6E+06	1.1E+06	1.2E+06	2.6E+06	3.1E+05	1.6E+05
752	6.2E+06	1.4E+06	6.1E+06	1.5E+06	2.1E+05	3.1E+05

			CcP_B			
I (mM)	**k(II)**	**st.dev.**	**k(III)**	**st.dev.**	**k(IV)**	**st.dev.**
44	1.4E+09	3.5E+08	1.4E+09	3.5E+08	1.8E+06	2.1E+06
122	2.0E+09	2.8E+08	2.0E+09	2.8E+08	2.1E+07	9.5E+06
192	7.5E+08	1.6E+08	7.5E+08	1.6E+08	1.1E+07	4.5E+06
292	2.2E+08	4.3E+07	2.2E+08	4.3E+07	1.9E+06	1.1E+06
392	6.2E+07	1.1E+07	5.7E+07	1.1E+07	1.6E+05	1.5E+05
502	2.8E+07	3.3E+06	2.8E+07	3.3E+06	1.9E+05	1.9E+05
622	1.4E+07	1.9E+06	1.1E+07	3.2E+06	3.1E+05	2.1E+05
752	6.7E+06	6.0E+05	7.5E+06	2.0E+06	3.0E+04	7.3E+04

			CcP_C			
I (mM)	**k(II)**	**st.dev.**	**k(III)**	**st.dev.**	**k(IV)**	**st.dev.**
44	3.1E+06	2.6E+05	1.2E+06	2.1E+05	7.6E+03	8.6E+03
122	1.0E+06	7.5E+04	-2.6E+04	5.8E+04	5.0E+04	2.2E+04
192	8.5E+05	8.9E+04	1.5E+05	6.9E+04	7.5E+04	1.9E+04
292	1.0E+06	8.6E+04	5.2E+05	1.6E+05	3.2E+04	1.3E+04
392	6.8E+05	9.3E+04	4.1E+05	1.8E+05	8.0E+03	1.1E+04
502	6.7E+05	4.9E+04	4.7E+05	6.9E+04	1.3E+04	7.4E+03
622	6.7E+05	4.9E+04	5.5E+05	1.3E+05	4.5E+03	6.4E+03
752	6.0E+05	7.6E+04	1.8E+05	5.7E+04	3.1E+04	1.4E+04

CcP_D						
I (mM)	**k(II)**	**st.dev.**	**k(III)**	**st.dev.**	**k(IV)**	**st.dev.**
44	1.1E+09	1.9E+08	6.6E+08	3.3E+08	5.2E+06	2.1E+06
122	1.4E+09	1.1E+08	1.4E+09	1.1E+08	8.0E+06	2.2E+06
192	7.8E+08	2.1E+08	3.8E+08	6.0E+07	6.8E+06	3.7E+06
292	1.7E+08	2.6E+07	1.0E+08	1.8E+07	4.3E+06	2.0E+06
392	5.8E+07	2.9E+06	5.4E+07	4.8E+06	6.8E+05	5.4E+05
502	2.5E+07	1.5E+06	2.0E+07	8.2E+05	6.8E+05	1.5E+05
622	1.4E+07	1.1E+06	1.2E+07	2.6E+06	9.4E+04	1.6E+05
752	7.2E+06	4.8E+05	4.2E+06	7.2E+05	6.4E+05	2.4E+05

CcP_E						
I (mM)	**k(II)**	**st.dev.**	**k(III)**	**st.dev.**	**k(IV)**	**st.dev.**
44	1.74E+06	1.60E+05	8.46E+05	1.60E+05	2.25E+04	2.2E+04
122	6.18E+05	1.67E+05	1.40E+04	8.64E+04	5.13E+04	2.2E+04
192	7.83E+05	8.81E+04	1.18E+05	5.12E+04	6.63E+04	1.9E+04
292	1.01E+06	1.37E+05	4.88E+05	3.00E+05	3.48E+04	1.4E+04
392	7.73E+05	7.64E+04	6.03E+05	1.24E+05	-2.29E+04	1.6E+04
502	6.15E+05	9.52E+04	2.60E+05	5.68E+04	3.08E+04	9.5E+03
622	5.69E+05	4.59E+04	2.46E+05	6.21E+04	4.11E+04	1.7E+04
752	4.74E+05	2.27E+04	1.95E+05	3.81E+04	4.38E+04	1.0E+04

CcP_F						
I (mM)	**k(II)**	**st.dev.**	**k(III)**	**st.dev.**	**k(IV)**	**st.dev.**
44	9.6E+05	7.3E+04	3.1E+05	8.0E+04	2.5E+04	9.4E+03
122	7.6E+05	5.3E+04	4.8E+04	6.2E+04	3.2E+04	1.1E+04
192	6.0E+05	5.2E+04	-4.1E+04	6.2E+04	3.5E+04	2.0E+04
292	9.3E+05	1.1E+05	3.6E+05	1.6E+05	3.4E+04	7.5E+03
392	7.7E+05	6.2E+04	3.7E+05	1.4E+05	2.6E+04	1.2E+04
502	7.2E+05	8.2E+04	1.7E+05	9.3E+04	2.8E+04	7.3E+03
622	6.5E+05	4.5E+04	2.9E+04	3.6E+04	1.9E+04	4.2E+03
752	5.2E+05	3.6E+04	2.0E+04	2.2E+04	2.9E+04	2.7E+03

Table S4.4. Association rate constants ($M^{-1}s^{-1}$) for the Cc:CcP_A complexes obtained by simulation and by fitting at ionic strength values from 44 mM to 752 mM. The error is calculated as standard deviation between the rates obtained by fitting or simulations of at least three single measurements at each ionic strength value.

		CcP_A	
		k_a	**st.dev.**
44 mM	**fitting**	1.5E+09	2.1E+08
	simulations	1.7E+09	3.2E+08
122 mM	**fitting**	1.5E+09	1.2E+08
	simulations	1.7E+09	3.6E+08
192 mM	**fitting**	6.8E+08	1.3E+08
	simulations	7.7E+08	9.7E+07
292 mM	**fitting**	1.5E+08	4.4E+06
	simulations	1.3E+08	1.9E+07
392 mM	**fitting**	4.5E+07	3.3E+06
	simulations	4.4E+07	5.8E+06
502 mM	**fitting**	2.4E+07	3.3E+06
	simulations	2.0E+07	2.0E+06
622 mM	**fitting**	1.2E+07	6.6E+05
	simulations	8.2E+06	1.1E+06
752 mM	**fitting**	6.2E+06	1.1E+06
	simulations	6.2E+06	1.4E+06

Table S4.5. p-values obtained from the t-test performed by comparing the rate of association (k(II)) of the Cc:CcP complexes at ionic strength values from 44 mM to 752 mM. The grey boxes indicate p-values > 0.01, meaning that the difference in the rates of association is considered not to be significant. Bonferroni correction was applied using $p < 0.05$ for individual comparisions and $n = 5$ for the number of comparisons for each variant.

I (mM)	CcP_A/CcP_B	CcP_A/CcP_C	CcP_A/CcP_D	CcP_A/CcP_E	CcP_A/CcP_F
752	3.3E-01	2.4E-08	4.6E-02	2.1E-08	2.2E-08
622	5.2E-05	1.1E-06	1.5E-07	1.0E-06	1.1E-06
502	2.3E-08	3.0E-12	5.4E-04	2.7E-12	3.0E-12
392	8.4E-05	9.6E-08	8.4E-04	9.7E-08	9.7E-08
292	1.3E-06	2.3E-12	5.9E-02	2.3E-12	2.3E-12
192	6.9E-01	1.8E-11	8.8E-01	1.8E-11	1.8E-11
122	7.6E-02	3.3E-06	5.8E-02	3.3E-06	3.3E-06
44	4.5E-02	1.3E-06	4.1E-04	1.2E-06	1.2E-06

I (mM)	CcP_B/CcP_C	CcP_B/CcP_D	CcP_B/CcP_E	CcP_B/CcP_F	CcP_C/CcP_D
752	1.1E-08	8.9E-02	1.4E-08	1.4E-08	1.0E-09
622	2.6E-07	7.2E-01	2.5E-07	2.6E-07	1.1E-17
502	2.6E-15	4.9E-02	2.4E-15	2.6E-15	6.2E-05
392	2.2E-12	1.4E-01	2.2E-12	2.2E-12	3.6E-05
292	6.9E-11	1.7E-02	6.9E-11	6.9E-11	1.1E-03
192	5.4E-09	6.9E-01	5.4E-09	5.4E-09	1.1E-06
122	1.9E-07	2.8E-04	1.9E-07	1.9E-07	6.5E-07
44	1.0E-05	6.7E-02	1.0E-05	1.0E-05	4.3E-09

I (mM)	CcP_C/CcP_E	CcP_C/CcP_F	CcP_D/CcP_E	CcP_D/CcP_F	CcP_E/CcP_F
752	2.3E-03	2.3E-02	1.7E-09	1.6E-09	1.4E-02
622	3.5E-04	5.5E-01	1.0E-17	1.0E-17	3.7E-03
502	1.6E-01	1.7E-01	6.0E-05	6.2E-05	3.1E-02
392	6.7E-02	5.3E-02	3.6E-05	3.6E-05	9.6E-01
292	6.3E-01	6.6E-02	1.1E-03	1.1E-03	4.1E-01
192	2.9E-01	3.2E-05	1.1E-06	1.1E-06	2.0E-02
122	9.1E-05	3.2E-04	6.5E-07	6.5E-07	6.2E-02
44	4.8E-08	2.1E-08	4.3E-09	4.2E-09	3.4E-07

Table S4.6. Number of independent simulations performed to calculate the rate constants k(II), k(III) and k(IV), and used in t-test.

I (mM)	CcP_A	CcP_B	CcP_C	CcP_D	CcP_E	CcP_E
752	12	8	8	8	10	8
622	7	8	8	16	14	6
502	12	16	8	4	8	8
392	8	15	7	4	8	12
292	14	14	8	4	4	6
192	12	12	8	10	4	13
122	8	8	5	6	8	4
44	8	8	8	11	8	10

Script S4.1. Script used to perform the simulations on GNU Octave[18] of the entire cycle of reactions for the six CcP variants to match the experimental data curves.

```
# Model:
# S(1) + E(2) k2<Kd>k1 ES(3) k4<Ke>k3 P(4) + E(2)
# Cc(Fe2+) (1) + CcPI (2) k1-> Cc(Fe3+) (3) + CcPII (4)
# Cc(Fe2+)  (1) + CcPII (4) k2 -> Cc(Fe3+)  (3) + CcP(Fe3+)  (5)
# CcPII (4) + CcPII (4) k3-> CcPI (2) + CcP(Fe3+)  (5)
# k1>=k2>k3
# Load data and adjust
data = csvread("kinetic_data.csv");
time = data(:,1);

# Set variables
num3 = columns(data);
prod = data(:,2: num3);
prod = prod+0.0929;  # adjust to match data and simulations on the y axes

# Define rates and differential equations (1000 = 10^9)
function xdot = f (x,t)
  k1 = 1230;
  k2 = k1;
  k3 = 13;
  xdot = zeros (5,1);
  xdot(1) = -k1*x(1)*x(2)-k2*x(1)*x(4);
  xdot(2) = -k1*x(1)*x(2)+k3*x(4)*x(4);
  xdot(3) = k1*x(1)*x(2)+k2*x(1)*x(4);
  xdot(4) = k1*x(1)*x(2)-k2*x(1)*x(4)-k3*x(4)*x(4);
```

```
  xdot(5) = k3*x(4)*x(4)+k2*x(1)*x(4);
endfunction;

x0 = [0.5; 0.5; 0; 0; 0];
t = logspace(-5,-1,1000);
y1 = lsode ("f", x0, time);
y2 = lsode ("f", x0, time);
res = (y2(:,1)/1000)* ε_Cc(Fe2+) +(y2(:,3)/1000)* ε_Cc(Fe3+) + (y2(:,5)/1000)* ε_CcP(Fe3+)
+(y2(:,2)/1000)* ε_CpdI +(y2(:,4)/1000)* ε_CpdII; #fill in the right ε for each species according
to the salt concentration

plc = y1;
time1 = time + 0.001;

# Plot the results
# Normal plot of data and simulated product curves
h = figure('Position',[300,250,1300,500], 'Paperorientation', "landscape", 'Paperposition',
[0.0 1.0 11.0 6.0]);
subplot (1, 2, 1);
plot (time, prod, "-r","linewidth", 2, time-0.0002, res,"-k", "linewidth", 1);
axis([0, 0.025, 0.085, 0.095]);

set(gca, "linewidth", 2, "fontsize", 12)
xlabel ("Time (s)", "fontsize", 12);
ylabel ("A_{416}", "fontsize", 12);

# Log plot of all elements for last concentration
subplot (1, 2, 2);
plot (time,plc,"linewidth", 1);
axis([0, 0.025, 0, 0.5]);

set(gca, "linewidth", 2, "fontsize", 12);
xlabel ("Time (s)");
ylabel ("Concentration (uM)");
legend ("Cc(Fe2+) ", "CcPI", " Cc(Fe3+) ", "CcPII", "CcP", "location", "east");

save result.txt plc
save time.txt time
```

References

(1) Goodin, D. B., Davidson, M. G., Roe, J. A., Mauk, A. G., and Smith, M. (1991) Amino-acid substitutions at tryptophan-51 of cytochrome *c* peroxidase - Effects on coordination, species preference for cytochrome *c*, and electron-transfer. *Biochemistry 30*, 4953–4962.

(2) Volkov, A. N., Worrall, J. A. R., Holtzmann, E., and Ubbink, M. (2006) Solution structure and dynamics of the complex between cytochrome *c* and cytochrome *c* peroxidase determined by paramagnetic NMR. *Proc. Natl. Acad. Sci. U. S. A. 103*, 18945–18950.

(3) Schilder, J., Lohr, F., Schwalbe, H., and Ubbink, M. (2014) The cytochrome *c* peroxidase and cytochrome *c* encounter complex: The other side of the story. *Febs Lett. 588*, 1873–1878.

(4) Di Savino, A., Foerster, J., La Haye, T., Blok, A., Timmer, M., Ullmann, M., and Ubbink, M. (2020) Efficient encounter complex formation and electron transfer to cytochrome *c* peroxidase with an additional, distant electrostatic binding site. *Angew. Chemie Int. Ed. 132*, 23239–23243.

(5) Teske, J. G., Savenkova, M. I., Mauro, J. M., Erman, J. E., and Satterlee, J. D. (2000) Yeast cytochrome *c* peroxidase expression in Escherichia *coli* and rapid isolation of various highly pure holoenzymes. *Protein Expr. Purif. 19*, 139–147.

(6) Pollock, W. B., Rosell, F. I., Twitchett, M. B., Dumont, M. E., and Mauk, A. G. (1998) Bacterial expression of a mitochondrial cytochrome *c*. Trimethylation of lys72 in yeast iso-1-cytochrome *c* and the alkaline conformational transition. *Biochemistry 37*, 6124–6131.

(7) Pelletier, H., and Kraut, J. (1992) Crystal structure of a complex between electron transfer partners, cytochrome *c* peroxidase and cytochrome *c*. *Science (80-.). 258*, 1748–1755.

(8) Brünger, A. T., and Karplus, M. (1988) Polar hydrogen positions in proteins: Empirical energy placement and neutron diffraction comparison. *Proteins Struct. Funct. Bioinforma. 4*, 148–156.

(9) Brooks, B. R., Bruccoleri, R. E., Olafson, B. D., States, D. J., Swaminathan, S., and Karplus, M. (1983) CHARMM: A program for macromolecular energy, minimization, and dynamics calculations. *J. Comput. Chem. 4*, 187–217.

(10) MacKerell, A. D., Bashford, D., Bellott, M., Dunbrack, R. L., Evanseck, J. D., Field, M. J., Fischer, S., Gao, J., Guo, H., Ha, S., Joseph-McCarthy, D., Kuchnir, L., Kuczera, K., Lau, F. T. K., Mattos, C., Michnick, S., Ngo, T., Nguyen, D. T., Prodhom, B., Reiher, W. E., Roux, B., Schlenkrich, M., Smith, J. C., Stote, R., Straub, J., Watanabe, M., Wiórkiewicz-Kuczera, J., Yin, D., and Karplus, M. (1998) All-atom empirical potential for molecular modeling and dynamics studies of proteins. *J. Phys. Chem. B 102*, 3586–3616.

(11) Schrödinger, L. The PyMOL molecular graphics system, Version 1.3.

(12) Jurrus, E., Engel, D., Star, K., Monson, K., Brandi, J., Felberg, L. E., Brookes, D. H., Wilson, L., Chen, J., Liles, K., Chun, M., Li, P., Gohara, D. W., Dolinsky, T., Konecny, R.,

Koes, D. R., Nielsen, J. E., Head-Gordon, T., Geng, W., Krasny, R., Wei, G. W., Holst, M. J., McCammon, J. A., and Baker, N. A. (2018) Improvements to the APBS biomolecular solvation software suite. *Protein Sci. 27*, 112–128.

(13) Foerster, J. M., Poehner, I., and Ullmann, G. M. (2018) MCMap - A computational tool for mapping energy landscapes of transient protein-protein interactions. *ACS Omega 3*, 6465–6475.

(14) Miller, M. A., Liu, R. Q., Hahm, S., Geren, L., Hibdon, S., Kraut, J., Durham, B., and Millett, F. (1994) Interaction domain for the reaction of cytochrome *c* with the radical and the oxyferryl heme in cytochrome *c* peroxidase compound I. *Biochemistry 33*, 8686–8693.

(15) Hahm, S., Miller, M. A., Geren, L., Kraut, J., Durham, B., and Millett, F. (1994) Reaction of horse cytochrome *c* with the radical and the oxyferryl heme in cytochrome *c* peroxidase compound-I. *Biochemistry 33*, 1473–1480.

(16) Coulson, A. F., Erman, J. E., and Yonetani, T. (1971) Studies on cytochrome *c* peroxidase. XVII. Stoichiometry and mechanism of the reaction of compound ES with donors. *J. Biol. Chem. 246*, 917–924.

(17) Ho, P. S., Hoffman, B. M., Kang, C. H., and Margoliash, E. (1983) Control of the transfer of oxidizing equivalents between heme iron and free radical site in yeast cytochrome *c* peroxidase. *J. Biol. Chem. 258*, 4356–4363.

(18) John W. Eaton, David Bateman, Søren Hauberg, and R. W. (2014) GNU Octave version 3.8.1 manual: a high-level interactive language for numerical computations. *Creat. Indep. Publ. Platf.* URL https://www.gnu.org/software/octave/doc/v5.2.0/

(19) Margoliash, E., and Frohwirt, N. (1959) Spectrum of horse-heart cytochrome *c*. *Biochem. J. 71*, 570–578.